(Received 13 August 2024, Accepted 27 September 2024, Scheduled 9 October 2024)

A Spaceborne Inverse Sliding Spotlight SAR for Nonuniform Scanned Scene

Yangyang Chen[1, 2, *], Wei Xu[1, 2], Pingping Huang[1, 2], Weixian Tan[1, 2], and Yaolong Qi[1, 2]

[1] *College of Information Engineering, Inner Mongolia University of Technology, Hohhot, China*
[2] *Inner Mongolia Key Laboratory of Radar Technology and Application, Hohhot, China*

ABSTRACT: Inverse sliding spotlight synthetic aperture radar (SAR) is not as high as sliding spotlight SAR in azimuth resolution. Its azimuth resolution is constant, and it cannot meet the needs of multiple different azimuth resolutions. In order to solve this problem, a spaceborne inverse sliding spotlight SAR for nonuniform scanned scene is proposed. The design of the proposed inverse sliding spotlight SAR includes two parts: the design of the adaptive azimuth beam steering law and the design of the imaging algorithm. In the first part, the design of the adaptive azimuth beam steering law is based on multiple specific azimuth resolution requirements and the parameters of scanned scene. In the second part, the design of the imaging algorithm for the proposed inverse sliding spotlight SAR consists of three steps: filtering processing, phase compensation and upsampling processing, and image formation. Compared with the conventional inverse sliding spotlight SAR, the proposed inverse sliding spotlight SAR can achieve different azimuth resolution requirements for scanning targets at different positions in the scanned scene. Finally, the correctness of the proposed inverse sliding spotlight SAR is verified by simulation experiment and UAV SAR experiment.

1. INTRODUCTION

Spaceborne sliding spotlight synthetic aperture radar (SAR) obtains high azimuth resolution by rotating the azimuth beam steering around a virtual rotation point, but the sliding spotlight SAR is limited by the swath [1–3]. The azimuth beam of the inverse sliding spotlight SAR adopts a backward-forward rotation mode, in the same scanning time, and its beam azimuth scanning range is higher than that of the sliding spotlight SAR and strip SAR. The types of targets in the scanned scene are also enriched, and the azimuth resolution requirements are increased. In order to meet the resolution requirements of multiple targets as far as possible, inverse sliding spotlight mode is studied [4]. Because of its large illumination range, it is applied in many fields [5–8]. However, the azimuth resolution of the inverse sliding spotlight SAR is not very good [9].

In order to improve the azimuth resolution of the inverse sliding spotlight SAR to achieve high resolution and wide swath imaging requirements, many scholars have studied inverse sliding spotlight SAR. A converse beam cross (CBC) sliding spotlight SAR and its data block back projection algorithm are proposed. By finding a unified sliding factor suitable for sliding spotlight SAR and CBC sliding spotlight SAR, combined with data block back projection algorithm, good azimuth resolution can be achieved [10]. An imaging algorithm for spaceborne-airborne bistatic SAR (SA-BiSAR) is proposed, and this mode requires the radar transmitter and receiver to work in the sliding spotlight mode and inverse sliding spotlight mode, respectively, which increases the beam-overlapping area. The imaging algorithm applied to this mode can achieve good azimuth resolution [11]. However, the azimuth resolution of the above mode is constant, which cannot meet the requirements of multi-resolution. Terrain Observation by Progressive Scans (TOPS) SAR can be seen as a combination of multiple inverse sliding spotlight SARs. TOPS SAR has a wider range swath and wider scanning area than a single inverse sliding spotlight SAR. In order to improve the azimuth resolution of the TOPS SAR, a multi-channel single-phase center multi-beam TOPS SAR is proposed, but this method cannot flexibly meet the requirements of different azimuth resolutions [12]. A new full-polarization spaceborne MIMO-TOPS high-resolution wide-swath mode is proposed, but its improved azimuth resolution is not flexible enough for the change of azimuth resolution required by TOPS SAR specific scanned scene [13, 14]. Similarly, Extended Terrain Observation by Progressive Scans (ETOPS) mode of burst pulse imaging is proposed, which improves the azimuth resolution of TOPS by increasing the extended pulse duration before and after the pulse duration, but its improved azimuth resolution is not flexible enough [15].

If the conventional inverse sliding spotlight SAR works in a scanned scene with nonuniform targets distribution, due to the nonuniform distribution of targets, the required azimuth resolution is not constant. At this time, the conventional inverse sliding spotlight SAR cannot meet the needs of all regions for azimuth resolution. So in order to make the azimuth resolution of the inverse sliding spotlight SAR more flexible, an inverse sliding spotlight SAR for nonuniform scanned scene is proposed. The proposed inverse sliding spotlight SAR for nonuniform scanned scene realizes the high-resolution requirements of special areas by the adaptive beam steering law. The design of adaptive beam steering law includes six steps: determination

* Corresponding author: Yangyang Chen (20221100118@imut.edu.cn).

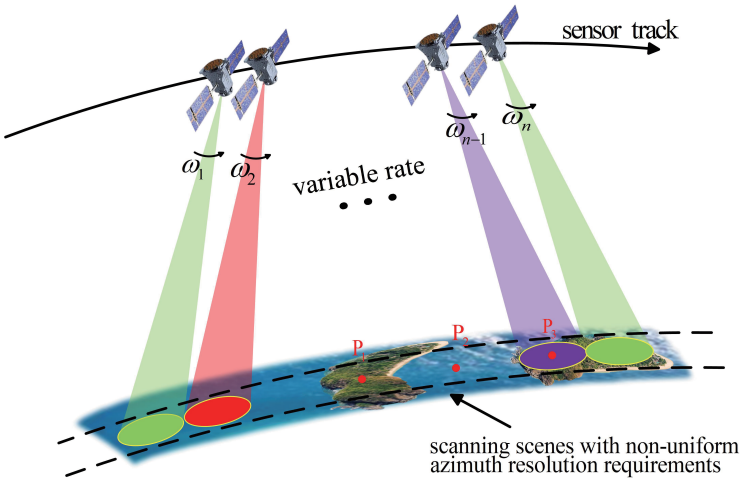

FIGURE 1. The scanning geometry model of the inverse sliding spotlight SAR for non-uniform scanning scene.

of the beam scanning angular velocity of targets, calculation of the targets scanning time, determination of the wave foot moving speed at the center time, calculation of the total scanning time, educing the fitting curve, and calculation of the number of resident pulses. Combined with the signal characteristics of the proposed inverse sliding spotlight SAR, an imaging algorithm is designed. The designed imaging algorithm includes three steps: filtering processing, phase compensation and upsampling processing, and image formation.

The structure of this paper is as follows. In the second section, the inverse sliding spotlight SAR for nonuniform scanned scene is proposed, and the adaptive azimuth beam steering law of the inverse sliding spotlight SAR for nonuniform scanned scene is designed. In the third section, the signal characteristics of the proposed inverse sliding spotlight SAR are analyzed, and the imaging algorithm is designed according to signal characteristics of the proposed inverse sliding spotlight SAR. In the fourth section, the correctness of the proposed inverse sliding spotlight SAR is verified by simulation experiment and unmanned aerial vehicle (UAV) SAR experiment. The fifth section is the summary.

2. INVERSE SLIDING SPOTLIGHT SAR FOR NON-UNIFORM SCANNED SCENE

2.1. The Inverse Sliding Spotlight SAR with Adaptive Azimuth Beam Steering

Inverse sliding spotlight SAR antenna beam steering law uses an inverse scanning method compared with a sliding spotlight SAR. The azimuth resolution of inverse sliding spotlight SAR can be expressed as:

$$\rho_a = \frac{L_a}{2}\left(\frac{\omega_r R_0}{v_g}+1\right) \tag{1}$$

where ω_r is the azimuth beam rotation rate, L_a the length of the azimuth antenna, v_g the actual wave foot moving speed along the ground of the inverse sliding spotlight SAR approximate plane geometry model, and R_0 the shortest distance from the radar to the ground.

The conventional inverse sliding spotlight SAR obtains the characteristics of wide azimuth swath at the expense of high resolution by the beam scans from back to front. Therefore, under the scanning characteristics of wide azimuth swath, the targets in the scanned scene of inverse sliding spotlight SAR may be more abundant. In the scanned scene where the density of targets is sparse, at this time, there is no need for any important information to be obtained in the whole scanned scene. Therefore, the inverse sliding spotlight SAR can be used to scan a wide imaging area where the density of targets is low. However, if the conventional inverse sliding spotlight SAR works in a nonuniform scanned scene, as shown in Fig. 1, there are two islands in different positions of the scanned scene, and the rest are the sea surface. Therefore, there is no information for the sea surface that needs to be obtained, and more information on the island is needed. If the conventional inverse sliding spotlight SAR is used, more information on the island cannot be obtained. At this time, the conventional inverse sliding spotlight SAR is sub-optimal. In order to solve this problem, an inverse sliding spotlight SAR for a nonuniform scanned scene is proposed. This mode can be well realized for different azimuth resolutions required at different positions in a nonuniform scanned scene.

For example, the scanned scene of Fig. 1 is a nonuniform scanned scene, and there are three targets in Fig. 1: P_1, P_2, P_3. P_1 and P_3 are on the land which have many targets, and P_2 is on the sea which has almost no target. Therefore, for the land where there are many targets, high azimuth resolution is required to better observe the targets in the area, and for the sea where there is no target to observe at all, high azimuth resolution is not required. The conventional inverse sliding spotlight SAR cannot meet the requirements of azimuth resolutions of targets P_1, P_2, P_3 at the same time. The proposed inverse sliding spotlight mode can achieve the azimuth resolution requirements of targets at different azimuth positions through the adaptive azimuth beam steering law. Therefore, the required

azimuth resolutions of targets P_1, P_2, P_3 can be realized during one-time beam scanning.

2.2. Adaptive Azimuth Beam Steering Design

The adaptive azimuth beam steering law design of the proposed inverse sliding spotlight SAR is divided into six steps: calculating the beam rotation rate required for the target position, determining the azimuth time, calculating the moving speed of the azimuth beam on the ground at the central time, calculating the total scanning time, fitting the azimuth beam rotation rate curve, and calculating the number of resident pulses required for the target position.

Firstly, according to the different azimuth resolution requirements $\rho_1, \rho_2, \ldots, \rho_n, \ldots, \rho_N$ by target points in the scanned scene, the required azimuth beam rotation rates $\omega_1, \omega_2, \ldots, \omega_n, \ldots, \omega_N$ respectively are expressed as:

$$\omega_n = \frac{v_g\left(2\rho_n - L_a\right)}{R_0 L_a} \tag{2}$$

Then, according to the azimuth positions $x_1, x_2, \ldots, x_n, \ldots, x_N$ of targets and the different required azimuth resolutions, the azimuth time $\eta_1, \eta_2, \ldots, \eta_n, \ldots, \eta_N$ of scanning targets can be determined.

After that, the moving speed of the azimuth beam on the ground at the central time can be expressed as:

$$v_{f,0} = v_g\left(\frac{\omega_c R_0}{v_g} + 1\right) \tag{3}$$

where ω_c is the azimuth beam rotation rate at the central time.

Then, the total scanning time of the proposed inverse sliding spotlight SAR can be obtained:

$$T = \frac{L + L_f}{v_{f,0}} \tag{4}$$

where L is the distance of the beam moving on the ground, and L_f is the length of the azimuth beam projected on the ground. The total scanning time range is obtained as $[-T/2, T/2]$.

After that, the varying curve of the azimuth beam scanning rate of the proposed inverse sliding spotlight SAR for nonuniform scanned scene is fitted by $(\eta_1, \omega_1), (\eta_2, \omega_2), \ldots, (\eta_n, \omega_n), \ldots, (\eta_N, \omega_N)$ which are obtained from the first step and second step. As shown in Fig. 2, when the number of target points is more than three, the quadratic fitting curve cannot meet the azimuth resolution requirements of all target points, and the cubic fitting curve can meet the azimuth resolution requirements of more target points at the same time. In order to meet the azimuth resolution requirements well and reduce the computation, take the cubic fitting curve. The equations used to fit the cubic curve can be expressed as:

$$\begin{cases} \omega_r(\eta) = \omega_c + a_1\eta + a_2\eta^2 + a_3\eta^3 \\ \omega_r(\eta_n) = \omega_n, n \in [1, 2, \ldots, N] \end{cases} \tag{5}$$

where a_1, a_2, a_3 are the coefficients of the fitting curve of azimuth beam rotation rate.

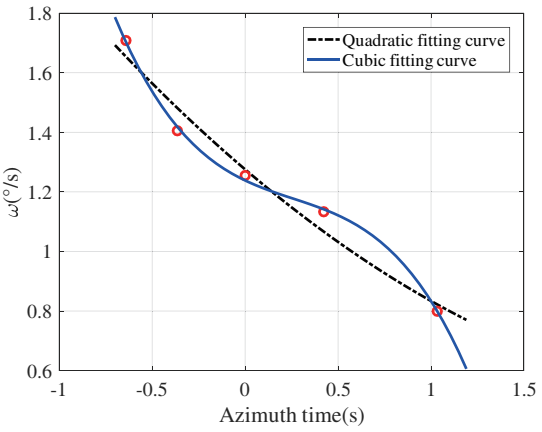

FIGURE 2. Comparison of two fitting curves.

Then, the number of resident pulses required for these target points $N_1, N_2, \ldots, N_n, \ldots, N_N$ under the scanning of the proposed inverse sliding spotlight SAR is obtained. The number of resident pulses can be calculated as:

$$N_n = \text{round}\left(\frac{q}{|\omega_r(\eta)|} \cdot \text{PRF}\right) \tag{6}$$

where round $(\cdot)$ is the rounding operator, PRF the pulse repetition frequency, and q the step angular interval for azimuth beam step scanning in the phased array antenna (PAA).

3. IMAGING ALGORITHM OF THE INVERSE SLIDING SPOTLIGHT SAR FOR NONUNIFORM SCANNED SCENE

3.1. Signal Analysis

The Doppler centroid frequency of the proposed inverse sliding spotlight SAR can be expressed as:

$$\begin{aligned} f_{dc}(\eta) &= \frac{2v_s f_c}{c}\sin\left[\theta(\eta)\right] \\ &\approx \frac{2v_s f_c}{c}\int \omega_r(\eta)d\eta \\ &\approx \frac{2v_s f_c}{c}\left(\omega_c\eta + \frac{a_1}{2}\eta^2 + \frac{a_2}{3}\eta^3 + \frac{a_3}{4}\eta^4\right) \end{aligned} \tag{7}$$

where f_c is the radar frequency, c the speed of light, v_s the radar platform speed, and $\theta(\eta)$ the azimuth beam steering angle.

Combining (5) with (7), the Doppler centroid varying rate of the proposed inverse sliding spotlight SAR is expressed as:

$$\begin{aligned} k_{rot}(\eta) &= \frac{\partial f_{dc}(\eta)}{\partial\eta} \\ &\approx \frac{2v_s f_c}{c}\left(\omega_c + a_1\eta + a_2\eta^2 + a_3\eta^3\right) \end{aligned} \tag{8}$$

According to (8), the total azimuth Doppler bandwidth B_{tot} of the proposed inverse sliding spotlight SAR can be expressed

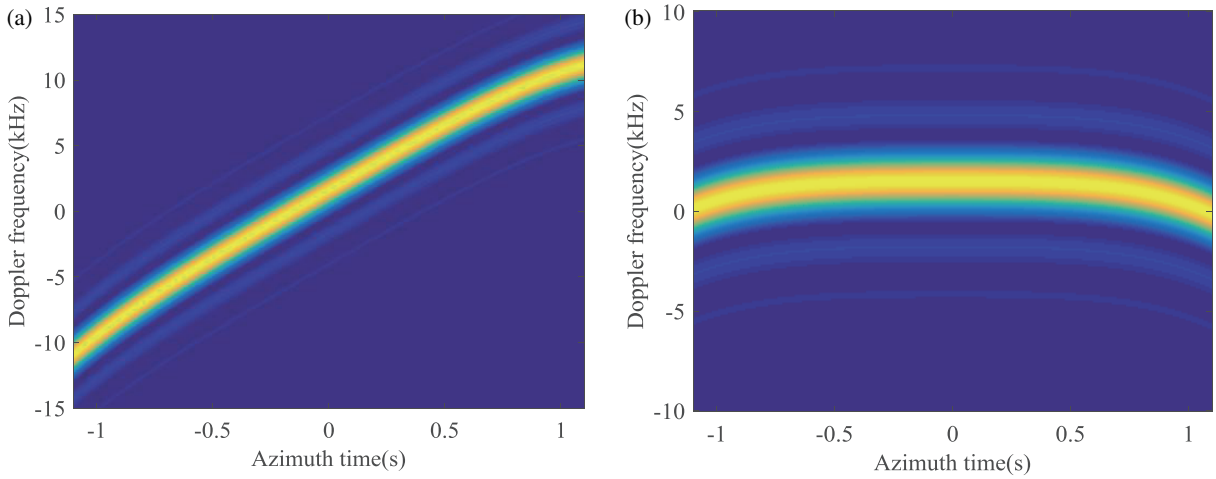

FIGURE 3. The azimuth time-frequency relationship diagram of the proposed inverse sliding spotlight SAR. (a) The initial azimuth time-frequency relationship diagram of the proposed inverse sliding spotlight SAR; (b) The azimuth time-frequency relationship diagram of the proposed inverse sliding spotlight SAR after traditional deramping method.

as:

$$\begin{aligned} B_{tot} &= B_f + B_{rot} \\ &= \frac{2v_s f_c \theta_a}{c} + \int_{-\frac{T}{2}}^{\frac{T}{2}} k_{rot}(\eta)\, d\eta \\ &= \frac{2v_s f_c}{c}\left(\theta_a + \omega_c T + \frac{a_2 T^3}{12}\right) \end{aligned} \tag{9}$$

where B_{rot} is the Doppler bandwidth caused by the azimuth beam steering, and B_f is the azimuth beam bandwidth.

Under the condition of simulation parameters such as Table 1, the time-frequency relationship diagram of the proposed inverse sliding spotlight SAR is shown in Fig. 3(a), and the total azimuth Doppler bandwidth is greater than the PRF of the SAR system, so Doppler aliasing will occur. The two-step processing is often used to eliminate this Doppler aliasing phenomenon [16]. The time-frequency relationship of the signal after deramping processing of the two-step processing is shown in Fig. 3(b). The total azimuth Doppler bandwidth after traditional deramping processing method is 4682 Hz, and it is still greater than the PRF of the SAR system. Therefore, Doppler aliasing will still occur, which is not convenient for subsequent imaging. The total azimuth Doppler bandwidth $B_{tot,1}$ after deramping processing can be expressed as:

$$\begin{aligned} B_{tot,1} &= B_f + B_{res} \\ &= \frac{2v_s f_c \theta_a}{c} + \int_{-\frac{T}{2}}^{\frac{T}{2}} k_{rot}(\eta)\, d\eta - k_{rot,0} T \\ &= \frac{2v_s f_c}{c}\left(\theta_a + \frac{a_2 T^3}{12}\right) \end{aligned} \tag{10}$$

where B_{res} is the residual Doppler centroid varying bandwidth after traditional deramping processing, and θ_a is the azimuth beam width.

From (10), it can also be seen that after the proposed inverse sliding spotlight SAR signal is processed by the traditional deramping processing method, and there is still a residual Doppler bandwidth B_{res} generated by azimuth beam steering. Therefore, it can be concluded that the traditional deramping processing is no longer suitable for the signal processing of the proposed inverse sliding spotlight SAR.

TABLE 1. Simulation parameter.

Parameter	Value
Relative platform velocity	7643 m/s
Satellite altitude	600 km
Azimuth beam width	0.33°
Pulse repetition frequency PRF	3052 Hz
Radar carrier frequency	9.875 GHz
Pulse bandwidth	100 MHz
Pulse duration	8 μs
Distance sampling frequency	120 MHz
Azimuth antenna length	6.2 m

3.2. Design of Imaging Algorithm

In order to better deal with the proposed inverse sliding spotlight SAR signal, an imaging algorithm is designed in this paper. The designed imaging algorithm is mainly divided into three steps, as shown in Fig. 4.

The imaging processing steps are as follows. The first step is filtration, and the filtering processing makes the signal energy concentrate at 3 dB beam width. The secondly step is phase compensation and upsampling processing, including Doppler centroid removal, reramping processing, convolution upsampling processing, and Doppler history recovery. The thirdly

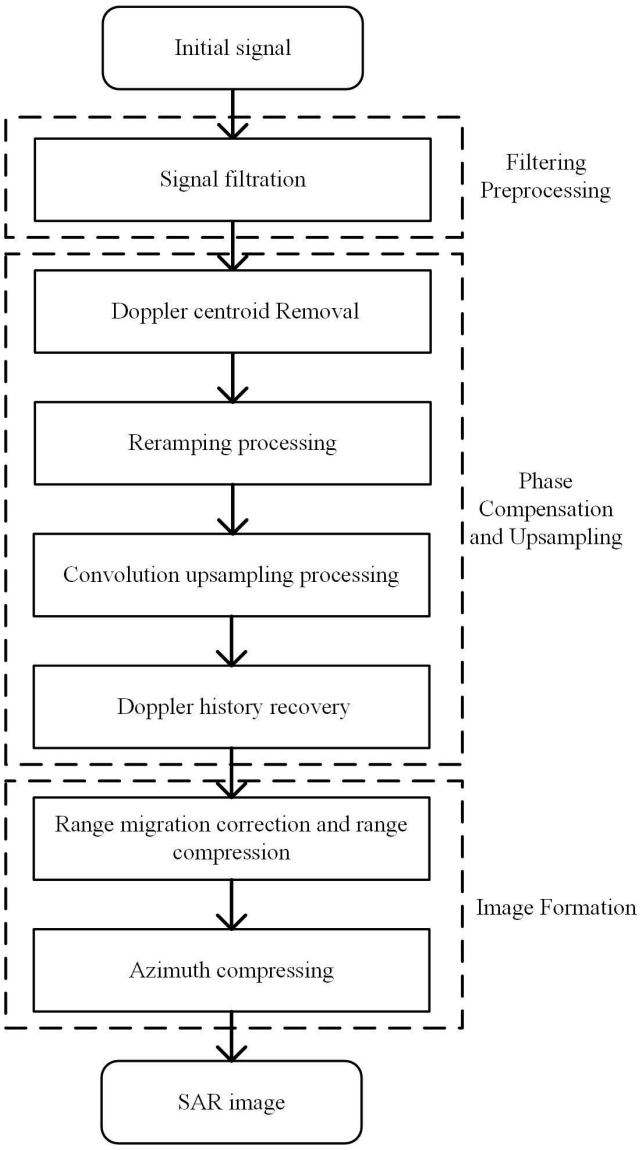

FIGURE 4. The flow chart of the designed imaging algorithm.

step is image formation, including range migration correction, range compression, and azimuth compression.

Firstly, In order to make the signal mainly concentrated in the beamwidth range, it is necessary to take a filtering processing to filter the signal outside the beamwidth range.

Then, the signal is processed by phase compensation and upsampling for subsequent accurate imaging. In order to completely eliminate the azimuth Doppler bandwidth caused by azimuth beam steering of the proposed inverse sliding spotlight SAR, the signal is multiplied by the Doppler centroid removal function. The Doppler centroid phase shift function can be expressed as:

$$h_1(\eta) = \exp\left\{\frac{-j4\pi v_s f_c}{c} \cdot \sin[\theta(\eta)] \cdot \eta\right\} \tag{11}$$

$$\approx \exp\left[\frac{-j4\pi v_s f_c}{c} \cdot \left(\omega_c \eta + \frac{a_1}{2}\eta^2 + \frac{a_2}{3}\eta^3 + \frac{a_3}{4}\eta^4\right) \cdot \eta\right]$$

At this time, the total azimuth Doppler bandwidth of the signal is less than the PRF of the SAR system.

After that, the signal is subjected to reramping processing. The reramping function can be expressed as:

$$h_2(\eta) = \exp\left[j\pi k_{ref}\eta^2\right] \tag{12}$$

with

$$k_{ref} = \frac{2v_s f_c}{c}\left(\omega_c + \frac{a_2}{12}T^2\right) \tag{13}$$

The sampling interval after convolution upsampling preprocessing should meet:

$$\frac{1}{\Delta\eta'} \geq B_{tot} \tag{14}$$

The numbers of azimuth sampling points N'_a after upsampling are updated to:

$$\begin{aligned} N'_a &= \left|\frac{1}{k_{ref}\cdot\Delta\eta'\cdot\Delta\eta}\right| \\ &= \frac{c}{2v_s f_c\left(\omega_c + \frac{a_2}{12}T^2\right)\cdot\Delta\eta'\cdot\Delta\eta} \end{aligned} \tag{15}$$

where $\Delta\eta$ is the sampling interval of the original signal. At this time, the signal has sufficient total sampling frequency in the azimuth direction for subsequent more accurate imaging.

In order to obtain more accurate imaging, the original Doppler history of the signal needs to be recovered. The original Doppler history recovery processing of the signal is realized by multiplying the signal after the convolution upsampling processing by a phase shift function, which can be expressed as:

$$\begin{aligned} h_3(\eta') \approx \exp\Bigg\{&\frac{j4\pi v_s f_c}{c}\left[\omega_c\cdot(\eta')^2 + \frac{a_1}{2}\cdot(\eta')^3\right. \\ &\left. + \frac{a_2}{3}\cdot(\eta')^4 + \frac{a_3}{4}\cdot(\eta')^5\right]\Bigg\} \end{aligned} \tag{16}$$

where $\eta' = N'_a \cdot \Delta\eta'$.

Finally, range migration correction, range compression, and azimuth compression are performed to obtain the initial SAR image.

4. SIMULATION

In this section, the effectiveness of the proposed inverse sliding spotlight mode is verified by Matlab simulation experiment and UAV SAR experiment. According to the parameters shown in Table 1, a design example of the proposed inverse sliding spotlight SAR for nonuniform scanned scene is given. In the simulation scene shown in Fig. 5(a), the azimuth resolution requirements of point targets P_1, P_2, P_3, P_4, and P_5 are respectively 10.89 m, 9.52 m, 8.89 m, 8.27 m, and 6.75 m. According to the specific azimuth resolution requirements, the required azimuth beam scanning rates of P_1, P_2, P_3, P_4, and P_5 are respectively: 1.707°/s, 1.404°/s, 1.255°/s, 1.134°/s, and 0.801°/s. The correlation curve is fitted by specific experiment, and the azimuth

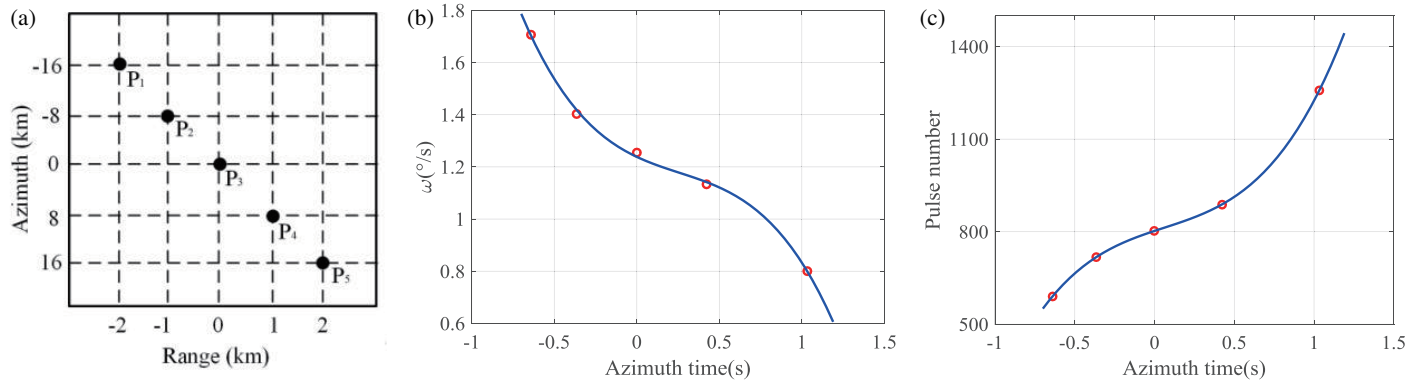

FIGURE 5. The simulation experience. (a) The simulation scene by design; (b) The adaptive azimuth beam steering curve; (c) The number of resident pulses curve.

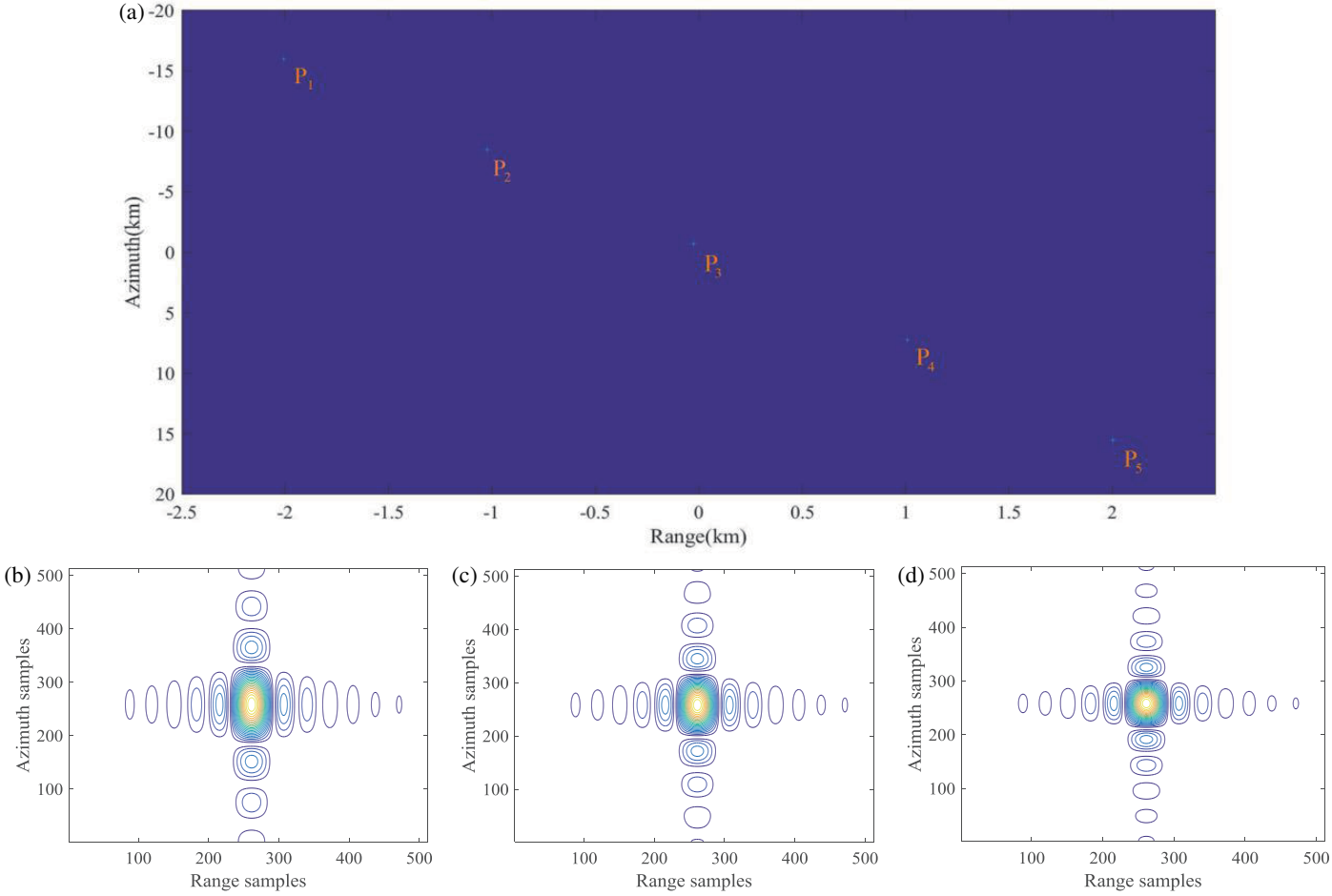

FIGURE 6. The simulation results of point targets. (a) The imaging results of five point targets; (b) Contour plots of P_1; (c) Contour plots of P_3; (d) Contour plots of P_5.

resolutions of P_1, P_2, P_3, P_4, and P_5 are respectively 10.913 m, 9.506 m, 8.876 m, 8.294 m, and 6.753 m, which is very close to the expected values. Through the specific design, the adaptive azimuth beam steering curve and the number of resident pulses curve are shown in the Figs. 5(b) and (c). It can be seen from Fig. 5(b) that as the requirements for azimuth resolution gradually increase, the rate of azimuth beam steering varying gradually slows down. It can be seen from Fig. 5(c) that as the azimuth resolution gradually increases, the number of resident pulses at each azimuth beam steering gradually increases.

The image shown in Fig. 6(a) is obtained by simulation. In order to better observe the focusing effect of P_1, P_3, and P_5, the contour plots of P_1, P_3, and P_5 are shown in Figs. 6(b)–(d). From the contour map of the three point targets, it can be

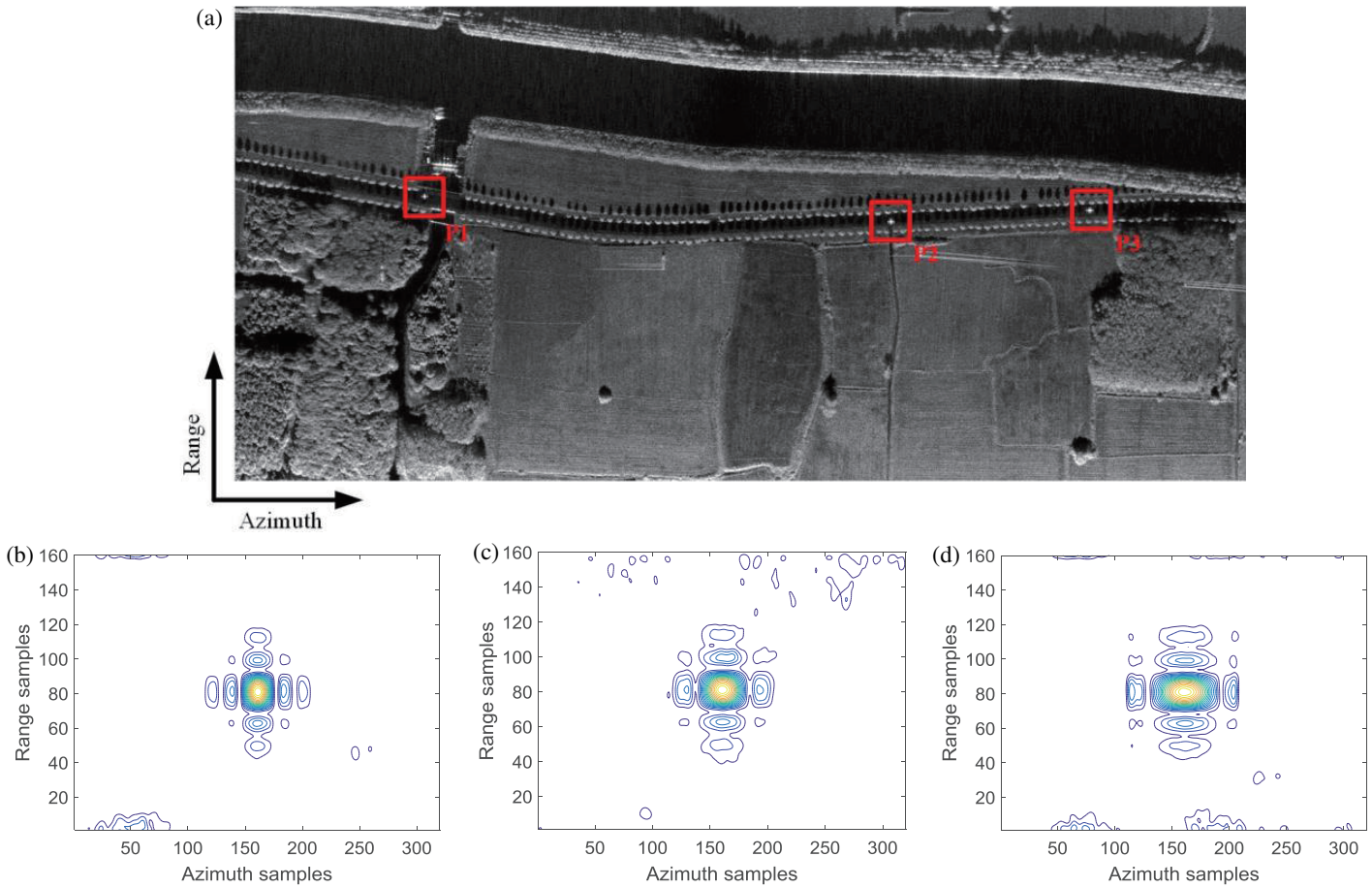

FIGURE 7. The results of UAV SAR experiment. (a) The imaging results of three point targets; (b) Contour plots of P_1; (c) Contour plots of P_2; (d) Contour plots of P_3.

seen that the focusing effect from point P_1 to point P_5 gradually becomes better, and the azimuth resolutions of P_1, P_3, and P_5 are close to the expected azimuth resolution requirements. These simulation experimental data confirm the correctness of the proposed inverse sliding spotlight mode.

In order to further verify the correctness of the proposed SAR scanning mode, a flight experiment is carried out by using a UAV SAR system with a very large azimuth width of the antenna beam. Then, the UAV SAR signal is combined with the azimuth time-frequency filtering to realize the adaptive beam steering law. The imaging results of the equivalent SAR raw data generated by the UAV SAR system data are shown in Fig. 7(a). It is assumed that the azimuth resolutions of P_1, P_2, and P_3 are reduced in turn. It can be seen from Fig. 7(a) that P_1, P_2, and P_3 all show excellent focusing effect.

In order to better observe the varying of the azimuth focusing effect of the target points P_1, P_2, and P_3, Figs. 7(b)–(d) are respectively the contour maps of the target points P_1, P_2, and P_3. From Figs. 7(b)–(d), it can be seen that the azimuth focusing effect of P_1 is significantly better than that of P_2 and P_3, and the azimuth focusing effects of P_1, P_2, and P_3 become worse in turn. Therefore, the azimuth resolutions of P_1, P_2, and P_3 gradually decrease, which meets the requirements of azimuth resolution.

5. CONCLUSION

This paper proposes an inverse sliding spotlight SAR for nonuniform scanned scene, which is mainly divided into two parts: the design of the adaptive beam steering law and imaging algorithm. In the nonuniform scanned scene, the proposed inverse sliding spotlight mode can well meet multiple azimuth resolution requirements that the conventional inverse sliding spotlight SAR cannot meet. Firstly, the adaptive azimuth beam steering law designs a specific adaptive azimuth beam steering through specific resolution requirements. Then, according to the signal characteristics of the proposed inverse sliding spotlight mode, an imaging algorithm suitable for this mode is designed. The imaging algorithm firstly takes a filtering process to filter the signal outside the beamwidth range; then, the Doppler bandwidth generated by the azimuth beam steering is eliminated, and reramping processing is performed; after that, the convolution upsampling processing is used to make the signal have sufficient sampling frequency; then, the original Doppler history of the signal is restored to facilitate subsequent accurate imaging; finally, imaging is performed by range migration correction, range compression, and azimuth compression. The results of simulation experiment and UAV SAR experiment show the flexibility of the proposed inverse sliding spotlight SAR in achieving azimuth resolution. In

summary, through the specific design, the proposed inverse sliding spotlight SAR realizes the specific requirements of different azimuth resolutions in nonuniform scanned scene and overcomes the limitations of the conventional inverse sliding spotlight SAR in azimuth resolution. In order to make the azimuth resolution more flexible and accurate, further research can be carried out on more flexible azimuth beam steering control strategy and its hardware implementation. In terms of hardware implementation, the design of phased array antenna and real-time control system can be used to realize the adaptive adjustment of beam steering, and the calculation task of beam adaptive steering can be realized by Digital Beamformer (DBF) and high-performance digital signal processor.

ACKNOWLEDGEMENT

This work was supported by the National Natural Science Foundation of China under grant numbers 62071258 and U22A2010.

REFERENCES

[1] Li, N., S. Niu, Z. Guo, Y. Liu, and J. Chen, "Raw data-based motion compensation for high-resolution sliding spotlight synthetic aperture radar," *Sensors*, Vol. 18, No. 3, 842, 2018.

[2] Dell'Aglio, D. A. G., G. D. Martino, A. Iodice, D. Riccio, and G. Ruello, "A unified formulation of SAR raw signals from extended scenes for all acquisition modes with application to simulation," *IEEE Transactions on Geoscience and Remote Sensing*, Vol. 56, No. 8, 4956–4967, 2018.

[3] Kuang, H., J. Chen, W. Yang, and W. Liu, "An improved imaging algorithm for spaceborne MAPs sliding spotlight SAR with high-resolution wide-swath capability," *Chinese Journal of Aeronautics*, Vol. 28, No. 4, 1178–1188, 2015.

[4] Yang, W., J. Chen, W. Liu, P. Wang, and C. Li, "A modified three-step algorithm for TOPS and sliding spotlight SAR data processing," *IEEE Transactions on Geoscience and Remote Sensing*, Vol. 55, No. 12, 6910–6921, 2017.

[5] Nannini, M., P. Prats-Iraola, F. D. Zan, and D. Geudtner, "TOPS time series performance assessment with TerraSAR-X data," *IEEE Journal of Selected Topics in Applied Earth Observations and Remote Sensing*, Vol. 9, No. 8, 3832–3848, 2016.

[6] Fan, H., Z. Zhang, R. Wang, N. Li, W. Xu, and Z. Xu, "Demonstration of dual-channel TOPS SAR imaging with airborne C-band data," *IEEE Journal of Selected Topics in Applied Earth Observations and Remote Sensing*, Vol. 10, No. 8, 3569–3581, 2017.

[7] Xu, L., Q. Chen, J.-J. Zhao, X.-W. Liu, Q. Xu, and Y.-H. Yang, "An integrated approach for mapping three-dimensional coseismic displacement fields from Sentinel-1 TOPS data based on DInSAR, POT, MAI and BOI techniques: Application to the 2021 mw 7.4 maduo earthquake," *Remote Sensing*, Vol. 13, No. 23, 4847, 2021.

[8] Duan, H., Y. Li, B. Li, and H. Li, "Fast InSAR time-series analysis method in a full-resolution SAR coordinate system: A case study of the Yellow River Delta," *Sustainability*, Vol. 14, No. 17, 10597, 2022.

[9] Bi, H., G. Li, Y. Song, J. Zhang, D. Zhu, W. Hong, and Y. Wu, "Design and performance analysis of sparse Tops SAR mode," *IEEE Journal of Selected Topics in Applied Earth Observations and Remote Sensing*, Vol. 15, 8898–8909, 2022.

[10] Yin, C.-B. and D. Ran, "Converse beam cross sliding spotlight SAR imaging processing with data-blocking based fast back projection," in *2016 IEEE International Geoscience and Remote Sensing Symposium (IGARSS)*, 1070–1073, Beijing, China, 2016.

[11] Yan, F. and W. Chang, "An efficient approach for double sliding spotlight bistatic synthetic aperture radar focusing," in *2015 8th International Congress on Image and Signal Processing (CISP)*, 732–736, Shenyang, China, 2015.

[12] Xu, W., P. Huang, and Y.-K. Deng, "Multi-channel SPCMB-tops SAR for high-resolution wide-swath imaging," *Progress In Electromagnetics Research*, Vol. 116, 533–551, 2011.

[13] Xu, W., P. Huang, and Y.-K. Deng, "MIMO-TOPS mode for high-resolution ultra-wide-swath full polarimetric imaging," *Progress In Electromagnetics Research*, Vol. 121, 19–37, 2011.

[14] Huang, P. and W. Xu, "ASTC-MIMO-TOPS mode with digital beam-forming in elevation for high-resolution wide-swath imaging," *Remote Sensing*, Vol. 7, No. 3, 2952–2970, 2015.

[15] Huang, P. and W. Xu, "A new spaceborne burst synthetic aperture radar imaging mode for wide swath coverage," *Remote Sensing*, Vol. 6, No. 1, 801–814, 2014.

[16] Zhu, D., T. Xiang, W. Wei, Z. Ren, M. Yang, Y. Zhang, and Z. Zhu, "An extended two step approach to high-resolution airborne and spaceborne SAR full-aperture processing," *IEEE Transactions on Geoscience and Remote Sensing*, Vol. 59, No. 10, 8382–8397, 2021.